Critical Spacing in Cell-Matrix Mechanical Feedback Controls Tissue Condensation

Xiangjun Peng[1,2], Yuxuan Huang[2], Elliot L. Elson[2,*], Guy M. Genin[2,*], and Xi-Qiao Feng[1,*]

[1]Department of Engineering Mechanics, Applied Mechanics Laboratory, Institute of Biomechanics and Medical Engineering, Tsinghua University, Beijing 100084, China
[2]NSF Science and Technology Center for Engineering Mechanobiology, Department of Mechanical Engineering and Materials Science, Washington University, St. Louis, MO, USA
[*]e-mail: elson@wustl.edu; genin@wustl.edu; fengxq@tsinghua.edu.cn

ABSTRACT

The mechanical interplay between cells and their extracellular matrix (ECM) presents a fundamental paradox in mechanobiology: while individual cells respond monotonically to increasing mechanical stimulus, collective cellular behaviors exhibit sharp transitions at critical cell densities. This is particularly evident in tissue condensation, where cell-seeded collagen matrices either dramatically contract or remain unchanged depending on whether the initial cell spacing falls below or above a critical threshold. Here we resolve this apparent contradiction through bio-chemo-mechanical modeling of cell-ECM interactions. We show that while increasing ECM stiffness enhances individual cell activation, it simultaneously weakens the mechanical cross-talk between cells, creating a non-monotonic relationship that governs collective behavior. This competition between local activation and neighbor communication establishes a critical spacing threshold below which cells can mechanically polarize their neighbors through ECM remodeling. The predicted critical spacing aligns with experimental observations of the cell density required for tissue condensation, reconciling single-cell and collective responses. Our model reveals how recursive interactions between cellular contractility and ECM mechanics give rise to emergent spatial ordering, demonstrating how complex multicellular behaviors can emerge from simple mechanical principles. These findings provide a physical basis for understanding mechanobiological signaling, with implications for tissue development and disease progression.

Mechanical interactions between neighboring cells and their extracellular matrix (ECM) are critical determinants of cellular behavior, driving processes such as wound healing, development, and fibrotic disease progression[1–5]. Fibroblasts are central players in these phenomena, as they can activate to exert the contractile forces on surrounding ECM that underlie tissue remodeling. These interactions form the basis of cell-to-cell communication through the ECM, a phenomenon that underlies a wide range of physiological and pathological processes[4,6]. Despite their fundamental importance, the mechanisms governing how cells interact with their neighbors and achieve contractility and ECM remodeling remain poorly understood.

Recent studies have established the concept of an optimal substrate stiffness for phenomena such as cell adhesion, traction generation, and migration[7–9]. However, the role of optimal stiffness in the context of cell-ECM feedback and fibroblast activation in physiological, fibrous ECM has not been investigated. Moreover, the activation of fibroblasts within collagen matrices is linked to the concept of a critical cell density, below which cells are unable to effectively activate one another and contract the ECM[5,10–12]. This paratensile signaling phenomenon is particularly relevant to fibrotic remodeling of soft tissues and to wound healing, but the underlying mechanisms remain unclear[4,6].

A relatively narrow range of conditions determine whether cells in a collagen hydrogel can succeed in activating their neighbors sufficiently to shrink the hydrogel substantially. Following Doha, et al.[5], we studied data indicating the degree to which cells compacted collagen gels as a function of initial cell spacing. The data of Marquez, et al.[10] suggest a critical cell density of $\phi_c = 400,000 - 500,000$ cells/ml for chick embryo fibroblasts in 1 mg/ml type I collagen, for a spacing $s_c = 1/\phi_c^{1/3}$ of $130 - 140$ μm (Supplemental Figure). Fernandez and Bausch report a critical area density of $0.0001 - 0.0002$ cells /μm^2 in 250 μm thick gels ($\phi_c = 400,000 - 800,000$ cells/ml) for MC3T3-E1 osteoblast cells in 2.4 mg/ml collagen, for $s_c = 110 - 140$ μm (Supplemental Figure). Doha, et al.[5] conducted definitive experiments characterizing this phenomenon. Their data show the beginnings of strong contraction at 250,000 NIH 3T3 fibroblast cells/ml, with contraction increasing to an asymptote at 2,000,000 cells/ml, yielding a range $s_c = 79 - 160$ μm in 2 mg/ml collagen. These effects are very general, with the distance between cells and the mechanical properties of collagen ECM significantly influence cells such as neurons as well[13].

To elucidate the mechanisms underlying these interactions, we developed an integrated bio-chemo-mechanical model that captures the recursive relationship between cell activation and stretch-driven ECM stiffening. This integrates models of stress-driven cell activation, which capture increases in myosin motor density and polarization in response to mechanical cues, and fiber recruitment models that describe ECM stiffening under strain[14–18]. The cell models capture how actomyosin

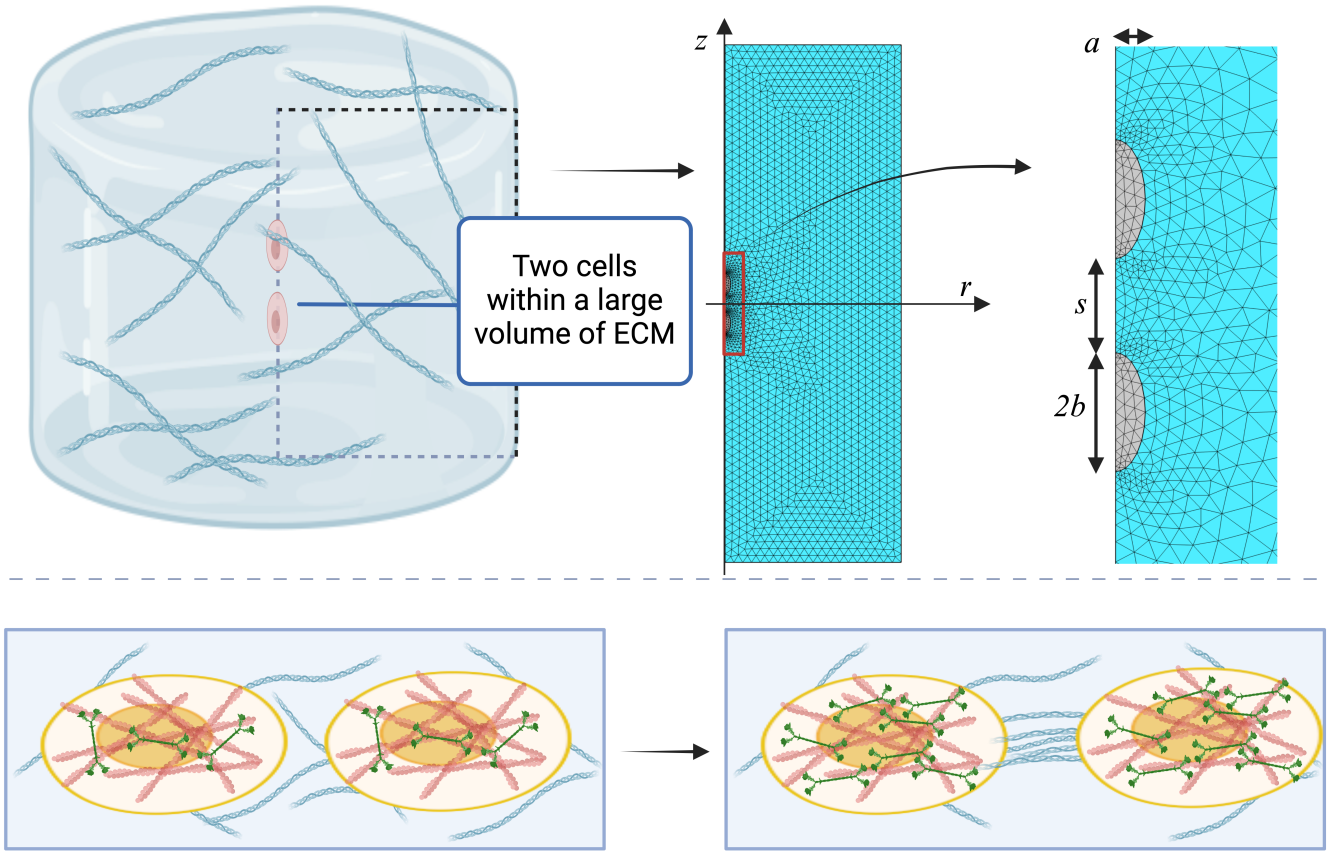

Figure 1. (top) A pair of ellipsoidal cells in a very large, fibrous extracellular matrix (ECM) were modeled. The finite element mesh was highly refined around the cells. (bottom) The active model for the cell accounted for how cells synthesize myosin motors in response to mechanical stress, and how they polarize. The ECM model accounted for fiber recruitment and alignment.

contractility and focal adhesion complexes affect cell signaling pathways to drive the evolution of subsequent remodeling of the actomyosin contractile apparatus[14]. The ECM models capture how collagen fibers both realign and stiffen in tension, but buckle in compression, which is a function of factors such as ECM fiber density and thickness that can vary with age and disease[19,20].

Our approach allows us to dissect how cell spacing and shape interact with ECM stiffness to determine how cells influence the contractility and polarization of their neighbors. This model provides insights into the mechanical basis for critical distances in paratensile signaling and into how cell aspect ratio and ECM properties jointly regulate force transmission in both health and disease.

By dissecting these mechanisms, our study not only fills a critical gap in understanding cellular interactions in fibrosis and wound healing but also offers new insights into how cell spreading facilitates long-range force transmission within tissues. These findings have implications for developing targeted interventions in fibrosis, cancer progression, and chronic wounds by manipulating the physical microenvironment to control cellular communication and tissue remodeling.

Fibroblasts can activate neighbors mechanically within a critical spacing

To identify how recursive cell-ECM interactions give rise to cell-cell mechanical communication, we combined a bio-chemo-mechanical model of fibroblasts with a nonlinear, strain-stiffening model of a fibrous ECM, and applied a computational implementation of this to model interactions between two ellipsoidal cells spaced a distance s apart axially within a much larger volume of ECM (Figure 1). The minor axes of the cells were $R = 10\mu$m. The contractile actomyosin machinery of the cells was modeled with a contractility tensor, $\boldsymbol{\rho}$, that evolved in response to the cell's mechanical microenvironment[14,16] (see *Methods and materials*). This evolution accounted for chemo-mechanical feedback through a "chemo-mechanical feedback parameter," α, representing the tendency to increase contractility in response to mechanical stress. It also accounted for the associated resistance to this increase in metabolic output, represented by the "chemical stiffness parameter," β (see *Methods and materials*). The ECM was represented by the fibrous continuum constitutive model of Wang, et al.[21], wherein the fibrous

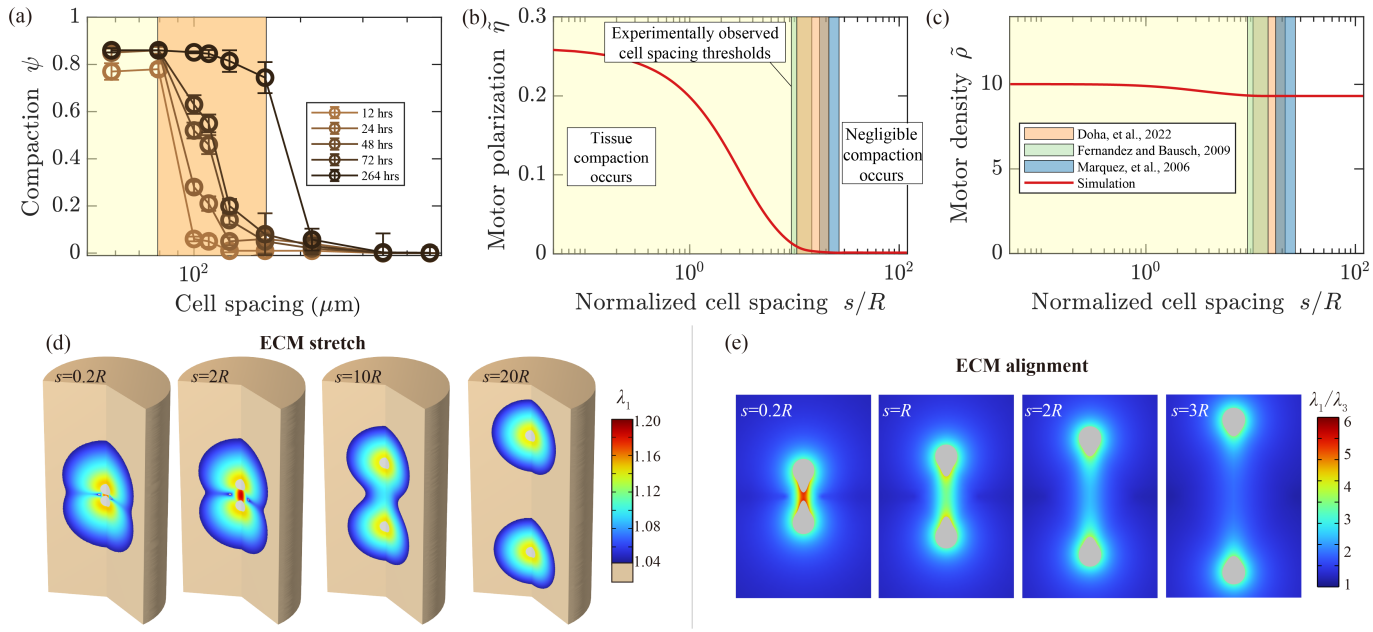

Figure 2. Cell can sense each other and compact ECM when spaced closer than a critical spacing. (a) The data of Doha, et al.[5] showing that the dimensionless degree of compaction ($\psi(t) = 1 - A(t)/A(t=0)$, where $A(t)$ is the area of a thin, button-shaped tissue construct at time t) increases dramatically for a cell spacing below a critical spacing of 79-160 μm. (b-c) Data from additional studies (see Supplemental Figure S1) show a critical spacing in this range as well. Here, spacing is normalized by a nominal cell radius of 10 μm for comparison to simulations (red lines). The critical spacing corresponds to the radius at which substantial polarization of myosin motors ($\tilde{\rho}$) occurs, but is only weakly dependent upon the density $\tilde{\rho}$ of myosin motors. (d) These forces are arise through recursive interactions with a fibrous ECM that stiffens when stretched beyond a critical stretch ratio, λ_c (here taken as 1.04). Cells spaced sufficiently far apart do not strain the ECM sufficiently to stiffen it. (e) ECM alignment (represented as the ratio between the first and third principal stretch ratios) drops stronly with increased spacing.Parameter values: $E^f/E^b = 50$, $\lambda_c = 1.04$, $\alpha = 2.4$ kPa^{-1}, $\beta = 2.5$ kPa^{-1}, $\rho_0 = 1$ kPa, $K = 0.833$ kPa, $\mu = 0.385$ kPa[16].

ECM is characterized by an elastic modulus E^b at low strain, and by transition to a strain-stiffening network for principal stretches beyond a critical value, λ_c.

Results shed light on ways that cells can become activated through mechanical interactions within their neighbors. As expected from numerous earlier studies[4–6,13,22,23], even spherical cells in sufficiently close proximity stretched and aligned the collagen between them (Figure 2d-e). This was evident as bands of highly aligned collagen, with fibers aligning along the contractile axis between cells, and buckling perpendicular to this, as evident from the ratio between the maximum and minimum principal stretch ratios (λ_1/λ_3) (Figure 2e)[15,20]. The spherical cells compacted spherical regions of ECM around them to levels beyond the critical stretch, taken here to be $\lambda_c = 1.04$, as is appropriate for collagen in the 1-2 mg/ml range[20,21]. For cells spaced apart a distance $s = 20R$, these regions of strain-stiffening collagen did not overlap, but for cells spaced more closely together, the collagen matrix aligned strongly in the characteristic tension bands that are broadly reported[4,5,13,20,23] (Figure 2d).

These effects were recursive, with the alignment and stiffening of the ECM leading to increasing activation of contractility in cells, and this contractility leading to further alignment of the ECM (REF Farid Nature Materials). We quantified these effects by considering two parameters, and analyzed them in the context of the extreme compaction of collagen when cells spacing is below the critical threshold (Figure 2b-c). The density of myosin motors, $\tilde{\rho} = \mathrm{tr}(\boldsymbol{\rho})/3$, increased very slightly below the critical spacing (Figure 2c). However, the key difference was in the polarization of myosin motors within the cell ($\tilde{\eta} = (\rho_1 - \rho_3)/2$, where ρ_1 and ρ_3 are the largest and smallest eigenvalues of $\boldsymbol{\rho}$, respectively. This changed dramatically at the critical spacing (Figure 2b). We therefore studied how cell-cell mechanical communication affected $\tilde{\eta}$ and $\tilde{\rho}$.

Myosin activation is determined by ECM properties alone, while cell polarization also depends upon cell spacing

To elucidate the mechanisms underlying these observations, we studied the joint effects on paratensile signaling of the cell spacing, s/R, and the pre-stiffening matrix modulus, E^b. We again studied spherical cells so as to capture the first stages of cell activation. As E^b increased, the zone of strain stiffening around the cells decreased and the tension band between them disappeared (Figure 3a). However, despite this diminishing alignment of ECM fibers, cell activation (motor density, $\tilde{\rho}$) increased monotonically and substantially with E^b (Figure 3b). The effect of cell spacing on $\tilde{\rho}$ was only a few percent, and extremely small compared to the variation with respect to E^b (Figure 3d).

The effect of stiffness on myosin motor polarization $\tilde{\eta}$ was much more substantial, with polarization disappearing beyond a critical spacing that diminished with increasing stiffness E^b (Figure 3c). The plateau signified the critical distance for mechanical communication between cells. The peak value of myosin motor polarization $\tilde{\eta}$ was a non-monotonic function of E^b. This maximum was determined by a trade-off between having a modulus sufficiently low for overlapping regions of ECM alignment to connect the cells, but sufficiently high to have substantial myosin motor activation, $\tilde{\rho}$ (Figure 3e). This balance thus determines how optimal stiffness arises through the effects on paratensile of cell spacing.

Cell spreading enhances mechanical feedback between cells and ECM

Because these results revealed a key role for actomyosin polarity, we next studied the polarization of shape that is characteristic of cell activation and spreading. An isolated cell with an aspect ratio of $b/a = 2$ in a very large ECM was modeled, with all parameters set at baseline level except the ECM modulus E^b. Volume was kept constant so that $a^2 b = R^3$. As with spherical cells, the zone around the cell for which the critical stretch ratio was exceeded shrank with increasing matrix modulus E^b (Fig. 4a). The displacement field was again a strong function of E^b (Fig. 4b). The myosin motor density $\tilde{\rho}$ was again a strong function of E^b, but only weakly dependent on b/a (Fig. 4c). Motor polarization $\tilde{\eta}$ was a much stronger function of modulus, E^b, with higher aspect ratio cells having higher motor polarization. The optimal stiffness for motor polarization decreased slightly with increasing aspect ratio (Fig. 4d).

Cell spreading and elongation enhances force transmission and mechanical communication

Results suggest that that cell aspect ratio significantly modulates force transmission and cell-cell mechanical communication through the ECM. Increasing cell aspect ratio (b/a) while holding cell volume constant led to an expansion of the volume of ECM stretched beyond the critical stretch ratio (Fig. 5). This resulted in a characteristic dumbbell-shaped zone of influence around elongated cells, indicating enhanced ECM deformation.

Both mean motor density ($\tilde{\rho}$) and mean motor polarization ($\tilde{\eta}$) increased as cells became more elongated (Fig.5b-c). This enhancement in myosin motor activity coincided with higher curvature at the ends of elongated cells, which creates localized stress concentrations. These stress concentrations, in turn, triggered a bio-chemo-mechanical feedback loop within the cell, leading to increased overall contractility and motor density.

The model also demonstrated increased force transmission by elongated cells. Both the first principal stress and displacement were transmitted further by cells with higher aspect ratios (Fig. 5d-e), potentially facilitating enhanced cell-cell communication through the ECM.

The spatial anisotropy of stress in elongated cells led to increased expression of phosphorylated myosin light chain and F-actin at the cell ends. This localized upregulation resulted in higher motor polarization, further contributing to the cell's exertion and transmission of forces. The strain-stiffening properties of the ECM amplified this effect, as the larger strains induced by elongated cells lead to increased local ECM stiffness.

Discussion

Cells in close proximity exhibited substantial activation of one another, polarizing the contractile machinery of neighboring cells. This interaction that weakened with increasing cell spacing until, beyond a critical distance, cells lost interconnectivity and become solely responsive to ECM properties.

Using a bio-chemo-mechanical model, we demonstrated the influence of physical properties such as cell distance, cell aspect ratio, and ECM stiffness on cell contractility, polarization, force transmission, and cell-cell mechanical communication. Results explain the existence of a critical distance below which cells can detect for paratensile signaling, and predict all existing experimental data for tissue condensation[5,10,11]. In a collective cell environment within the collagen matrix, this critical distance plays a pivotal role in facilitating the transition from disorder to order[5], and in the paratensile progression of fibrosis[4].

Our findings also reveal that the cell elongation and spreading enhance force transmission. Elongated cells exhibit stress concentrations at the ends, where surface curvature is high. This effect of anisotropy on contraction has been similarly

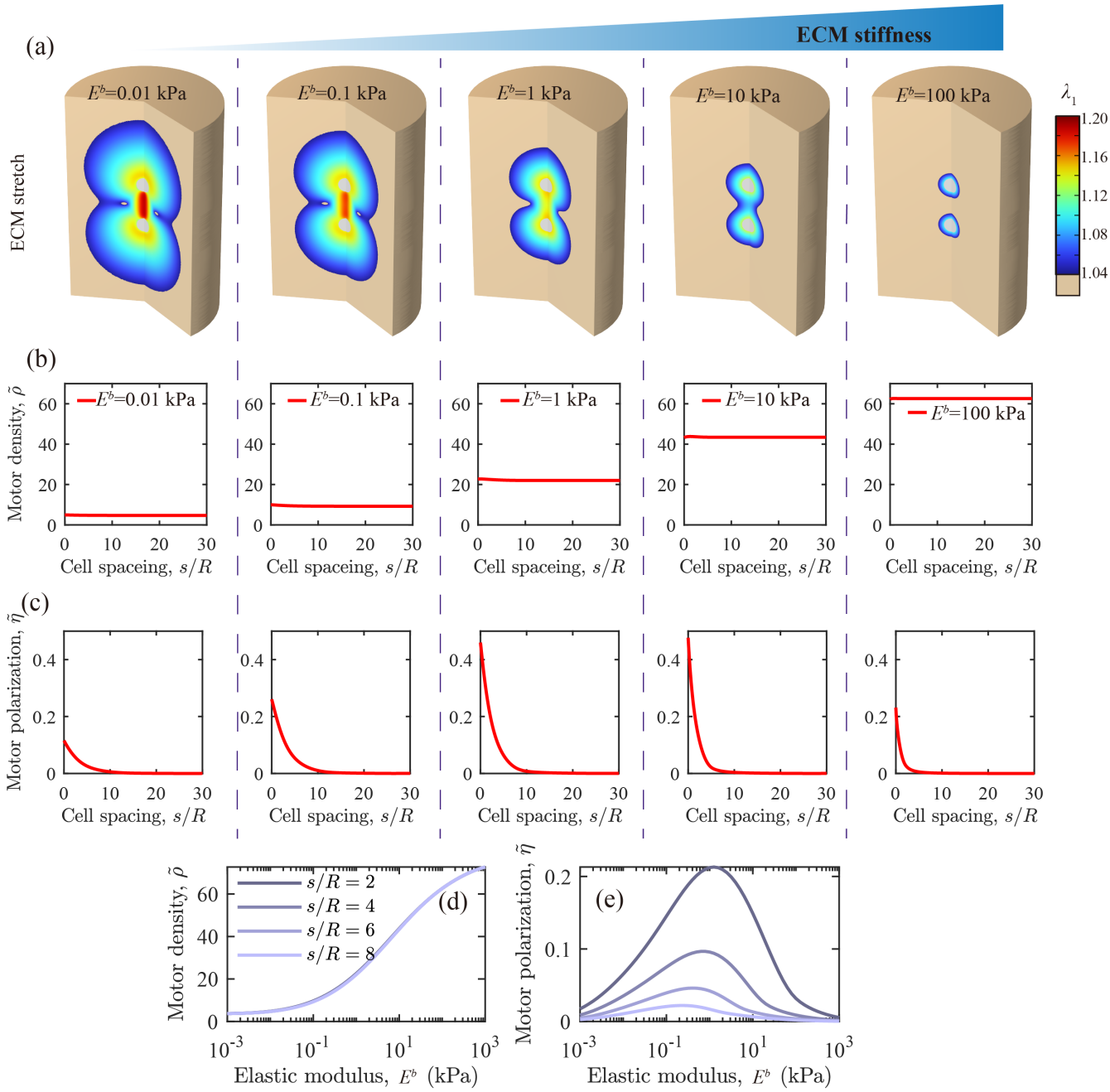

Figure 3. Effects of extracellular matrix (ECM) properties and cell spacing on paratensile signaling. (a) Strain stiffening zones and tension bands between spherical cells as a function of pre-stiffening matrix modulus (E^b), for cell spacing $s/R = 4$. (b) Myosin motor density ($\tilde{\rho}$) increases with E^b, showing minimal dependence on s/R. (c) Myosin motor polarization ($\tilde{\eta}$) as a function of E^b and s/R, demonstrating a critical spacing threshold that decreases with increasing E^b. (d) Comparison of $\tilde{\rho}$ variation with respect to E^b and s/R, demonstrating the substantial effect of E^b on $\tilde{\rho}$, and the very minor effect of s/R on $\tilde{\rho}$. (e) Peak $\tilde{\eta}$ as a function of E^b and s/R, illustrating the trade-off between ECM alignment and myosin motor activation in the determination of optimal stiffness for cell polarization and paratensile signaling. Parameter values: $E^f/E^b = 50$, $\lambda_c = 1.04$, $\alpha = 2.4\ \text{kPa}^{-1}$, $\beta = 2.5\ \text{kPa}^{-1}$, $\rho_0 = 1$ kPa, $K = 0.833$ kPa, $\mu = 0.385$ kPa[16].

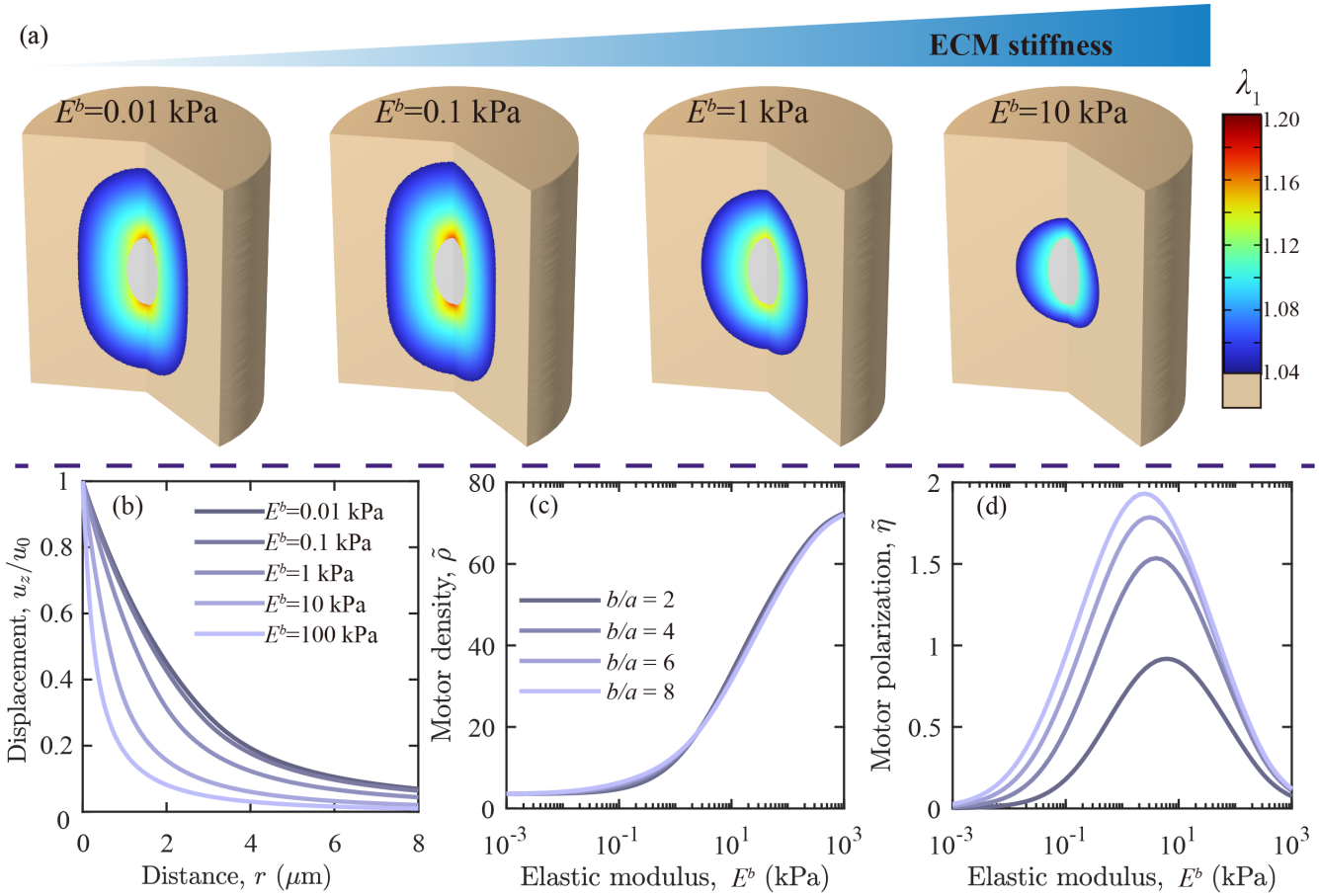

Figure 4. Effect of ECM stiffness on activation and polarization of an elongated, isolated cell. (a) Critical stretch ratio zone around an elongated cell (aspect ratio $b/a = 2$) for varying ECM moduli E^b. (b) Displacement field as a function of E^b. (c) Myosin motor density $\tilde{\rho}$ versus E^b and b/a. (d) Motor polarization $\tilde{\eta}$ as a function of E^b for different cell aspect ratios, showing optimal stiffness for polarization. Parameter values: $E^f/E^b = 50$, $\lambda_c = 1.04$, $\alpha = 2.4$ kPa^{-1}, $\beta = 2.5$ kPa^{-1}, $\rho_0 = 1$ kPa, $K = 0.833$ kPa, $\mu = 0.385$ kPa[16]

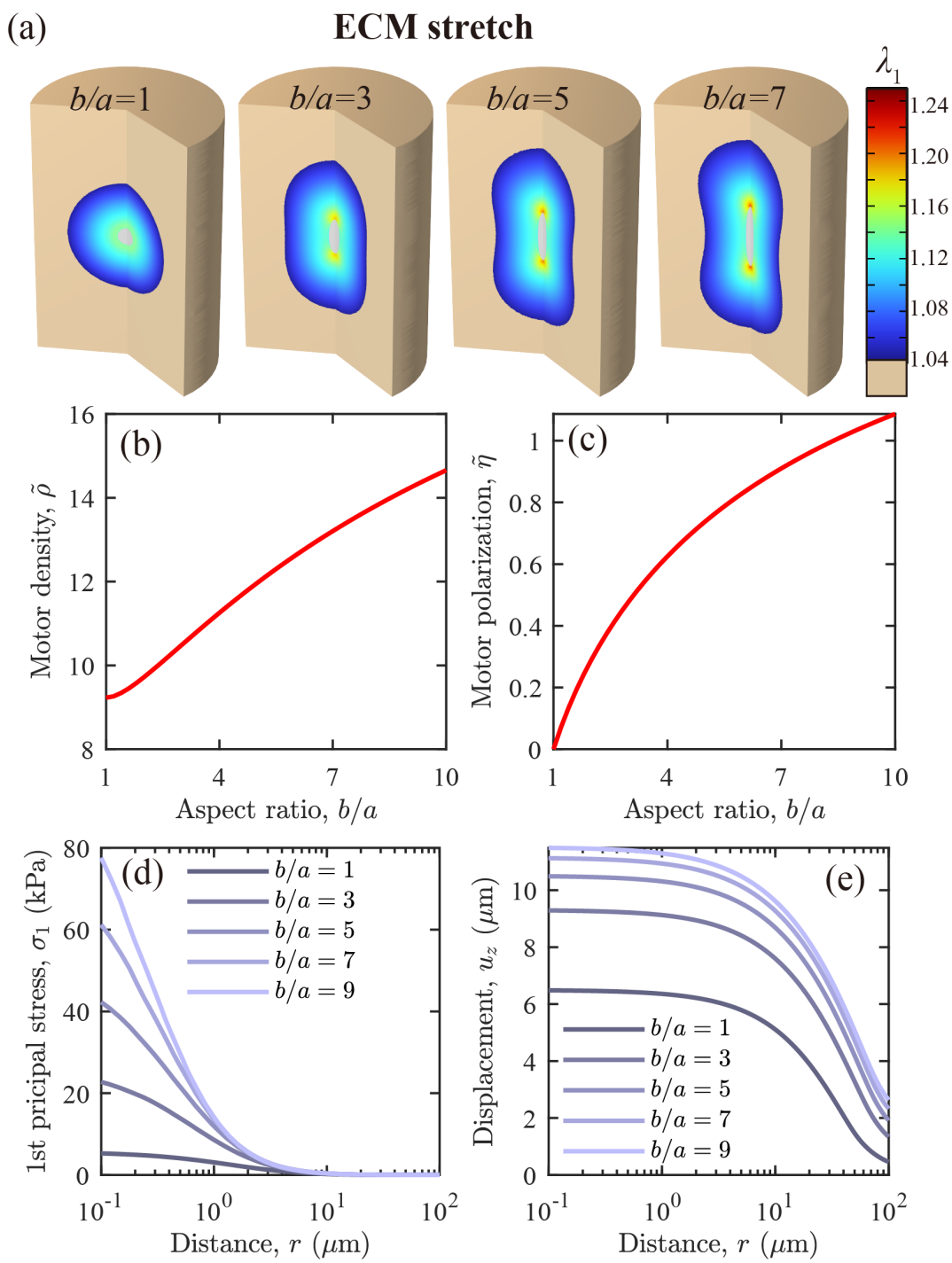

Figure 5. Cell aspect ratio modulates force transmission and mechanical communication. (a) Volume of ECM stretched beyond the critical stretch ratio increases with cell aspect ratio (a/b), showing a dumbbell-shaped zone of influence for elongated cells. (b) Mean myosin motor density ($\tilde{\rho}$) and (c) mean motor polarization ($\tilde{\eta}$) increase with rising cell aspect ratio. (d) First principal stress and (e) displacement fields demonstrate enhanced force transmission for cells with higher aspect ratios. Color scales represent normalized values, with warmer colors indicating higher magnitudes. Results illustrate how cell elongation amplifies cell-ECM interactions and facilitates long-range force transmission, potentially enhancing cell-cell mechanical communication. Parameter values: $E^b = 0.1$ kPa, $E^f/E^b = 50$, $\lambda_c = 1.04$, $\alpha = 2.4$ kPa^{-1}, $\beta = 2.5$ kPa^{-1}, $\rho_0 = 1$ kPa, $K = 0.833$ kPa, $\mu = 0.385$ kPa[16]

observed in 2D experimental studies[14]. More polarized cells can exert stronger contraction, allowing for extended transmission of mechanical signals. This suggests that cells such as fibroblasts that polarize engage in more efficient long-range force transmission and cell-cell mechanical communication when they do so. However, our model also suggests a non-monotonic relationship between ECM stiffness and cell polarization, implying the existence of an optimal ECM rigidity for effective cell-ECM interactions. This phenomenon has parallels in cell migration[9] and spreading[24] observed on 2D substrates.

Results showed that cell-ECM interactions are dominated by the low strain ECM stiffness. This activation can be transmitted to neighboring cells through paratensile signaling only if cell-cell communication is cell induces polarity. An isotropic cell can become polarized if the ECM rigidity is suitable to initiate cell activation and transmit sufficient mechanical stimuli to neighboring cells, thereby disrupting the isotropic distribution of myosin motors.

Our findings reveal a complex interplay between ECM properties, cell spacing, and cellular mechanical responses that governs paratensile signaling. The existence of an optimal ECM stiffness for cell polarization, coupled with a critical cell spacing threshold, provides a mechanistic explanation for the spatial limits of cell-cell communication observed in experiments[5,10,11]. This balance between ECM compliance and stiffness may be a key factor regulating tissue homeostasis and pathological processes like fibrosis. The differential effects of ECM properties on myosin motor density and polarization suggest that cells can modulate their response to mechanical cues through distinct mechanisms. This feedback loop can be further amplified by cell elongation. These insights could inform strategies for controlling cell behavior in tissue engineering applications and offer new avenues for therapeutic interventions in fibrotic diseases by targeting the mechanical microenvironment.

The bio-chemo-mechanical model demonstrates how cell distance, aspect ratio, and ECM stiffness influence cell contractility, polarization, and force transmission, thus facilitating intercellular mechanical communication. These findings have implications for understanding cellular behavior in physiological and pathological contexts, including wound healing and fibrosis, and underscore the importance of the physical microenvironment in cellular communication.

1 Conclusions

Cells in close proximity exhibit substantial activation of one another, leading to tissue condensation[5]. We show here that this can be explained via mechanical feedback mediated by the ECM. This paratensile interaction decreased with increasing cell spacing until, beyond a critical distance, cells lost their ability to communicate mechanically and responded exclusively to local ECM properties. This critical spacing emerges from competition between two opposing effects: ECM stiffness enhances individual cell activation but weakens cell-cell mechanical communication.

Bio-chemo-mechanical modeling demonstrated how this critical spacing depends on physical properties including ECM stiffness and cell aspect ratio. Our results explain the sharp transition in tissue condensation observed experimentally, with the predicted critical spacing matching all existing experimental data across different cell types and collagen densities. Cell elongation and spreading enhance force transmission by effectively extending the critical spacing: elongated cells exhibit stress concentrations at their ends, leading to enhanced local ECM remodeling. This suggests that cellular processes that drive elongation, such as fibroblast activation, can actively modulate the range of mechanical communication. However, this effect competes with ECM stiffness, resulting in a non-monotonic relationship between matrix rigidity and the ability of cells to communicate mechanically.

Results suggest physical principles governing how cells coordinate their behavior through ECM remodeling. The existence of a critical spacing, emerging from the competition between local activation and mechanical communication, provides a mechanistic framework for understanding both normal tissue development and pathological processes like fibrosis

References

1. Park, S. *et al.* Tissue-scale coordination of cellular behaviour promotes epidermal wound repair in live mice. *Nat. cell biology* **19**, 155–163 (2017).
2. Jiang, S. *et al.* An ex vivo culture model of kidney podocyte injury reveals mechanosensitive, synaptopodin-templating, sarcomere-like structures. *Sci. Adv.* **8**, eabn6027 (2022).
3. Chen, Y.-P. *et al.* Substrate nesting guides cyst morphogenesis of human pluripotent stem cells without 3d extracellular matrix overlay. *Acta Biomater.* **170**, 519–531 (2023).
4. Liu, L. *et al.* Matrix-transmitted paratensile signaling enables myofibroblast–fibroblast cross talk in fibrosis expansion. *Proc. Natl. Acad. Sci.* **117**, 10832–10838 (2020).
5. Doha, U. *et al.* Disorder to order transition in cell-ecm systems mediated by cell-cell collective interactions. *Acta Biomater.* **154**, 290–301 (2022).
6. Long, Y., Niu, Y., Liang, K. & Du, Y. Mechanical communication in fibrosis progression. *Trends Cell Biol.* **32**, 70–90 (2022).

7. Bangasser, B. L. *et al.* Shifting the optimal stiffness for cell migration. *Nat. communications* **8**, 15313 (2017).
8. Elosegui-Artola, A. *et al.* Mechanical regulation of a molecular clutch defines force transmission and transduction in response to matrix rigidity. *Nat. cell biology* **18**, 540–548 (2016).
9. Isomursu, A. *et al.* Directed cell migration towards softer environments. *Nat. materials* **21**, 1081–1090 (2022).
10. Marquez, J. P., Genin, G. M., Pryse, K. M. & Elson, E. L. Cellular and matrix contributions to tissue construct stiffness increase with cellular concentration. *Annals biomedical engineering* **34**, 1475–1482 (2006).
11. Fernandez, P. & Bausch, A. R. The compaction of gels by cells: a case of collective mechanical activity. *Integr. biology* **1**, 252–259 (2009).
12. Marquez, J. P., Elson, E. L. & Genin, G. M. Whole cell mechanics of contractile fibroblasts: relations between effective cellular and extracellular matrix moduli. *Philos. Transactions Royal Soc. A: Math. Phys. Eng. Sci.* **368**, 635–654 (2010).
13. Xie, R. *et al.* Fibrous viscoelastic extracellular matrix assists precise neuronal connectivity. *Adv. Funct. Mater.* 2301926 (2023).
14. Alisafaei, F., Jokhun, D. S., Shivashankar, G. & Shenoy, V. B. Regulation of nuclear architecture, mechanics, and nucleocytoplasmic shuttling of epigenetic factors by cell geometric constraints. *Proc. Natl. Acad. Sci.* **116**, 13200–13209 (2019).
15. Alisafaei, F., Chen, X., Leahy, T., Janmey, P. A. & Shenoy, V. B. Long-range mechanical signaling in biological systems. *Soft matter* **17**, 241–253 (2021).
16. Shenoy, V. B., Wang, H. & Wang, X. A chemo-mechanical free-energy-based approach to model durotaxis and extracellular stiffness-dependent contraction and polarization of cells. *Interface focus* **6**, 20150067 (2016).
17. Peng, X., Huang, Y. & Alisafaei, F. Cytoskeleton-mediated alterations of nuclear mechanics by extracellular mechanical signals. *Biophys. J.* **121**, 1–3 (2022).
18. Peng, X., Huang, Y. & Genin, G. M. The fibrous character of pericellular matrix mediates cell mechanotransduction. *J. Mech. Phys. Solids* **180**, 105423 (2023).
19. Lyu, C. *et al.* Advanced glycation end-products as mediators of the aberrant crosslinking of extracellular matrix in scarred liver tissue. *Nat. Biomed. Eng.* 1–18 (2023).
20. Hall, M. S. *et al.* Fibrous nonlinear elasticity enables positive mechanical feedback between cells and ecms. *Proc. Natl. Acad. Sci.* **113**, 14043–14048 (2016).
21. Wang, H., Abhilash, A., Chen, C. S., Wells, R. G. & Shenoy, V. B. Long-range force transmission in fibrous matrices enabled by tension-driven alignment of fibers. *Biophys. journal* **107**, 2592–2603 (2014).
22. Kollmannsberger, P., Bidan, C. M., Dunlop, J. W., Fratzl, P. & Vogel, V. Tensile forces drive a reversible fibroblast-to-myofibroblast transition during tissue growth in engineered clefts. *Sci. advances* **4**, eaao4881 (2018).
23. Ban, E. *et al.* Mechanisms of plastic deformation in collagen networks induced by cellular forces. *Biophys. journal* **114**, 450–461 (2018).
24. Zemel, A., Rehfeldt, F., Brown, A. E., Discher, D. E. & Safran, S. A. Optimal matrix rigidity for stress-fibre polarization in stem cells. *Nat. physics* **6**, 468–473 (2010).

Acknowledgements

X.P. and X.-Q.F. acknowledge support from Natural Science Foundation of China (Grants 11921002, 12402364 and 12032014). GMG acknowledges support from the National Institutes of Health (XXX, pending approval), and the Human Frontier Science Program (HFSP-RGP016/2024).

Author contributions

XP and YH performed simulations; all authors interpreted data; XP and GMG wrote the manuscript; all authors edited the manuscript.

Competing interests

The authors declare no competing interests.

Supplementary information

Model of cell contractility and activation

Cells were modeled as actively contracting and adapting ellipsoids embedded in an initially random, fibrous ECM that was very large compared to the cell. Actomyosin contractility was modeled as a directionally-distributed field of myosin force dipoles that contract an isotropic background of actin filaments[14]. Following Shenoy, et al.[16], this was represented by the contractility tensor, $\boldsymbol{\rho}$, derived by integrating forces from myosin dipoles over their orientation distribution. $\boldsymbol{\rho}$ is work conjugate to the linearized strain tensor, $\boldsymbol{\varepsilon}$, so that the specific work (per unit volume) done by phosphorylated myosin motors is $W = \boldsymbol{\rho} : \boldsymbol{\varepsilon}$. Cellular contractility developed in response to tension exposure, resulting in increased F-actin polymerization and elevated levels of phosphorylated myosin light chain (p-MLC), as represented by evolution of $\boldsymbol{\rho}$ evolved with tension[14]. The enthalpic state of the cell was represented by five terms[16]:

$$U = U_{\text{elastic}} - W_{\text{ext}} + U_{\text{chem}} - W_{\text{feedback}} + W_{\text{chem}} \tag{1}$$

where the strain energy density is:

$$U_{\text{elastic}} = \frac{K}{2} v^2 + \mu(\boldsymbol{e} : \boldsymbol{e}), \tag{2}$$

in which K is the cell's bulk modulus, $\boldsymbol{\varepsilon}$ is the infinitesimal strain tensor, $v = tr(\boldsymbol{\varepsilon})$ is the trace of $\boldsymbol{\varepsilon}$, μ is the shear modulus of the cell, and $\boldsymbol{e} = \boldsymbol{\varepsilon} - \frac{1}{3} v \boldsymbol{I}$ is the deviatoric portion of the strain tensor, in which $\boldsymbol{I}$ is the second order identity tensor. The external specific work was written:

$$W_{\text{ext}} = \int_0^v p\, dv + \int_0^{\boldsymbol{e}} \boldsymbol{s} : d\boldsymbol{e}, \tag{3}$$

in which $\boldsymbol{\sigma}$ is the linearized stress tensor, $p = \frac{1}{3}\text{tr}(\boldsymbol{\sigma})$, and $\boldsymbol{s} = \boldsymbol{\sigma} - p\boldsymbol{I}$ is the deviatoric component of the linearized stress tensor. The chemical energy density associated with phosphorylated myosin motors was written:

$$U_{\text{chem}} = 3\frac{\beta}{2}(p_m - \rho_o)^2 + \frac{\beta}{2}\boldsymbol{\rho}^{dev} : \boldsymbol{\rho}^{dev}, \tag{4}$$

in which $p_m = \frac{1}{3} tr(\boldsymbol{\rho})$, ρ_o is the baseline contractility, $\boldsymbol{\rho}^{dev} = \boldsymbol{\rho} - p_m \boldsymbol{I}$ is the deviatoric component of $\boldsymbol{\rho}$, and β is a constant termed the "chemical stiffness." Cells respond to mechanical stress by increasing $\boldsymbol{\rho}$, as governed by the feedback-associated specific work:

$$W_{\text{feedback}} = 3\alpha \int_0^{3p_m} p\, dp_m + \alpha \int_0^{\boldsymbol{\rho}^{dev}} \boldsymbol{s} : d\boldsymbol{\rho}^{dev}, \tag{5}$$

in which the constant α is the chemo-mechanical feedback parameter. Finally, the specific work done by the myosin motors was:

$$W_{\text{chem}} = 3p_m v + \boldsymbol{\rho}^{dev} : \boldsymbol{e}. \tag{6}$$

The temporal evolution equations can be inferred by taking time derivatives of Eq. 1[16]. For the cases of interest in which the timescales associated with motor recruitment and activation are short compared to the observation time, the following steady state conditions govern the active cell responses to mechanical stress:

$$\boldsymbol{\rho} = (\bar{\rho}_o + 3K^{\rho} v)\boldsymbol{I} + 2\mu^{\rho}\boldsymbol{e} \tag{7}$$

$$\boldsymbol{\sigma} = (\bar{\rho}_o + 3K^{e} v)\boldsymbol{I} + 2\mu^{e}\boldsymbol{e} \tag{8}$$

where $\overline{\rho}_o = \gamma\beta\rho_o$, $K^e = \gamma(K\beta - 1/3)$, $\mu^e = \gamma(\mu\beta - 1/2)$, $K^{\rho} = \gamma(K\alpha - 1/3)$, and $\mu^{\rho} = \gamma(\mu\alpha - 1/2)$, in which $\gamma = 1/(\beta - \alpha)$.

Model of fibrous ECM mechanics

We modeled the fibrous ECM using the approach of Wang, et al.[21], which treats the fibrous ECM as a superposition of elastic ground material and a set of fibers that provide additional resistance to deformation after stretching beyond a critical stretch level, λ_c. The total strain energy density of the collagen network is $U = U_b + U_f$, where the strain energy density associated with the ground material follows a neo-Hookean model:

$$U_b = \frac{\mu^b}{2}\left(\frac{\lambda_1^2+\lambda_2^2+\lambda_3^2}{J^{2/3}} - 3\right) + \frac{K^b}{2}(J-1)^2 \tag{9}$$

in which $\mu^b = E^b/(2(1+\nu^b))$ is the initial shear modulus, $K^b = E^b/(3(1-2\nu^b))$ is the initial bulk modulus, and E^b and ν^b are the initial elastic modulus and Poisson ratio of the ECM, respectively; $\{\lambda_1, \lambda_2, \lambda_3\}$ are the principal stretches; and $J = \lambda_1\lambda_2\lambda_3$. The strain energy density associated with aligned fibers is:

$$U_f = E^f \sum_{i=1}^{3} f_{ECM}(\lambda_i) \tag{10}$$

where E^f is a strain-stiffening modulus, and the dimensionless strain-stiffening function $f_{ECM}(\lambda_i)$ captures two fundamental principles: (*i*) the ECM exhibits strain stiffening solely in the direction of the first principal stretch when the stretch ratio exceeds a critical value λ_c, and (*ii*) effects of strain stiffening are negligible for stretch less than λ_c. From this, the stress in the matrix can be written as the sum of the stress in the ground material and the stress in the fiber network, $\boldsymbol{\sigma}^{ECM} = \boldsymbol{\sigma}^b + \boldsymbol{\sigma}^f$, where[21]:

$$\boldsymbol{\sigma}^b = K(J-1)\boldsymbol{I} + \mu\overline{\boldsymbol{B}}^{dev}/J \tag{11}$$

in which $\overline{\boldsymbol{B}}^{dev} = (\boldsymbol{B} - \frac{1}{3}\mathrm{tr}(\boldsymbol{B}))/J^{2/3}$ is the deviatoric part of the left modified Cauchy-Green tensor[21]. Here, $\boldsymbol{B} = \boldsymbol{F}\boldsymbol{F}^T = \sum_{i=1}^{3}\lambda_i^2(\boldsymbol{n}_i \otimes \boldsymbol{n}_i)$, where $\boldsymbol{F}$ is the deformation gradient tensor, λ_i $(i = 1,2,3)$ are the principal stretch ratios, and principal directions $\boldsymbol{n}_i$ are the unit eigenvectors of $\boldsymbol{B}$. Following[15,21], the contribution to fiber stiffening was written:

$$\boldsymbol{\sigma}^f = \frac{E_f}{J}\sum_{i=1}^{3}\frac{\partial f(\lambda_i)}{\partial \lambda_i}\lambda_i(\boldsymbol{n}_i \otimes \boldsymbol{n}_i) \tag{12}$$

where:

$$\frac{\partial f(\lambda_i)}{\partial \lambda_i} = \begin{cases} 0, & \lambda_i \le \lambda_p \\ \frac{(\lambda_i-\lambda_p)^{n+1}}{(\lambda_q-\lambda_p)^n(n+1)}, & \lambda_p \le \lambda_i \le \lambda_q \\ \frac{(1+\lambda_i-\lambda_q)^{m+1}-1}{m+1} + \frac{\lambda_q-\lambda_p}{n+1}, & \lambda_i \ge \lambda_q \end{cases} \tag{13}$$

in which $\lambda_p \equiv \lambda_c - \lambda_t/2$, $\lambda_q \equiv \lambda_c + \lambda_t/2$, λ_c is the stretch ratio at which fiber stiffening begins to contribute strongly to ECM mechanics, and λ_t is a transition region. For and strain-stiffening exponents m and n are fitting parameters[15,20].

Numerical methods

Equations were solved using the finite element in the COMSOL Multiphysics (COMSOL, Inc., Burlington, MA) environment. Cells were treated as axisymmetric. Cells and ECM were discretized with linear, triangular elements. Mesh convergence studies were performed, and convergence was typically achieved in models with approximately 100000 elements.

COMSOL's Solid Mechanics Interface (a component of the Structural Mechanics Module) was adopted to model the cross-talk between cells and ECM. Cell responses included passive and active components. The passive component was modeled as linear elastic. The active contractile stress, $\boldsymbol{\rho}$, was superimposed on the cell. To capture the presence of the two distinct families of aligned and isotropic fibers, a neo-Hookean model was adopted to capture the isotropic response, while Eq. 12 was used to include the contribution due to the aligned fibers.

Supplemental Figure

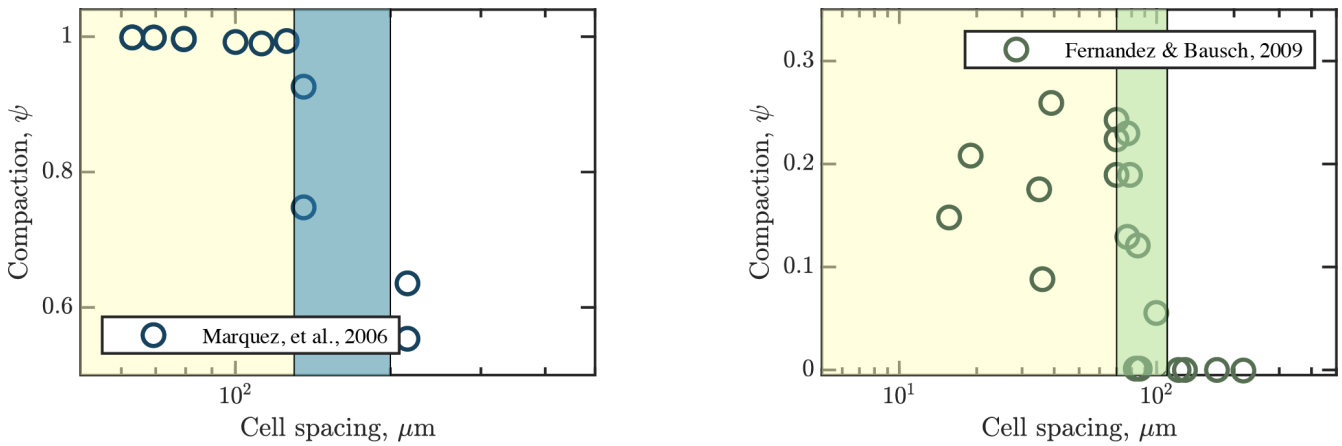

Figure S1. (Left) The data of Marquez, et al.[10] suggest a critical cell density of $\phi_c = 400,000 - 500,000$ cells/ml for chick embryo fibroblasts in 1 mg/ml type I collagen, for a spacing $s_c = 1/\phi_c^{1/3}$ of 130-140 μm. (Right) Fernandez and Bausch[11] report a critical area density of 0.0001-0.0002 cells /μm^2 in 250 μm thick gels ($\phi_c = 400,000 - 800,000$ cells/ml) for MC3T3-E1 osteoblast cells in 2.4 mg/ml collagen, for $s_c =$ 110-140 μm.